Comparison of human septal nuclei MRI measurements using automated segmentation and a new manual protocol based on histology

Tracy Butler, Laszlo Zaborszky, Elizabeth Pirraglia, Jinyu Li, Xiuyuan Hugh Wang, Yi Li, Wai Tsui, Delia Talos, Orrin Devinsky, Izabela Kuchna, Krzysztof Nowicki, Jacqueline French, Rubin Kuzniecky, Jerzy Wegiel, Lidia Glodzik, Henry Rusinek, Mony J. DeLeon, Thomas Thesen

PII: S1053-8119(14)00281-X
DOI: doi: 10.1016/j.neuroimage.2014.04.026
Reference: YNIMG 11282

To appear in: *NeuroImage*

Accepted date: 6 April 2014

Please cite this article as: Butler, Tracy, Zaborszky, Laszlo, Pirraglia, Elizabeth, Li, Jinyu, Wang, Xiuyuan Hugh, Li, Yi, Tsui, Wai, Talos, Delia, Devinsky, Orrin, Kuchna, Izabela, Nowicki, Krzysztof, French, Jacqueline, Kuzniecky, Rubin, Wegiel, Jerzy, Glodzik, Lidia, Rusinek, Henry, DeLeon, Mony J., Thesen, Thomas, Comparison of human septal nuclei MRI measurements using automated segmentation and a new manual protocol based on histology, *NeuroImage* (2014), doi: 10.1016/j.neuroimage.2014.04.026

Comparison of human septal nuclei MRI measurements using automated segmentation and a new manual protocol based on histology.

Tracy Butler[a,b], Laszlo Zaborszky[c], Elizabeth Pirraglia[a,] Jinyu Li[a], Xiuyuan Hugh Wang[b], Yi Li[a], Wai Tsui[a], Delia Talos[b], Orrin Devinsky[b], Izabela Kuchna[d], Krzysztof Nowicki[d], Jacqueline French[b], Rubin Kuzniecky[b], Jerzy Wegiel[d], Lidia Glodzik[a], Henry Rusinek[a], Mony J. DeLeon[a], Thomas Thesen[b]

a. Center for Brain Health
Department of Psychiatry
New York University School of Medicine
145 East 32nd Street
New York, NY 10016
USA

b. Comprehensive Epilepsy Center
Department of Neurology
New York University School of Medicine
223 East 34th Street
New York, NY 10016
USA

c. Center for Molecular and Behavioral Neuroscience
Rutgers, The State University of New Jersey
197 University Avenue
Newark, NJ 07102
USA

d. Institute for Basic Research in Developmental Disabilities
1050 Forest Hill Road
Staten Island, NY 10314
USA

Corresponding author:
Tracy Butler
Tracy.butler@nyumc.org
646 248 6734
New York University School of Medicine
Center for Brain Health, Department of Psychiatry
Comprehensive Epilepsy Center, Department of Neurology
145 East 32nd Street
New York, NY 10016

Abstract

Septal nuclei, located in basal forebrain, are strongly connected with hippocampi and important in learning and memory, but have received limited research attention in human MRI studies. While probabilistic maps for estimating septal volume on MRI are now available, they have not been independently validated against manual tracing of MRI, typically considered the gold standard for delineating brain structures. We developed a protocol for manual tracing of the human septal region on MRI based on examination of neuroanatomical specimens. We applied this tracing protocol to T1 MRI scans (n=86) from subjects with temporal epilepsy and healthy controls to measure septal volume. To assess the inter-rater reliability of the protocol, a second tracer used the same protocol on 20 scans that were randomly selected from the 72 healthy controls. In addition to measuring septal volume, maximum septal thickness between the ventricles was measured and recorded. The same scans (n=86) were also analysed using septal probabilistic maps and Dartel toolbox in SPM. Results show that our manual tracing algorithm is reliable, and that septal volume measurements obtained via manual and automated methods correlate significantly with each other ($p<.001$). Both manual and automated methods detected significantly enlarged septal nuclei in patients with temporal lobe epilepsy in accord with a proposed compensatory neuroplastic process related to the strong connections between septal nuclei and hippocampi. Septal thickness, which was simple to measure with excellent inter-rater reliability, correlated well with both manual and automated septal volume, suggesting it could serve as an easy-to-measure surrogate for septal volume in future studies. Our results call attention to the important though understudied human septal region, confirm its enlargement in temporal lobe epilepsy, and provide a reliable new manual delineation protocol that will facilitate continued study of this critical region.

Highlights

- Septal nuclei are important in memory but likely understudied
- We developed and tested a new manual tracing protocol to estimate septal size on MRI
- Manual and automated (SPM) septal volumes were correlated, but not identical
- Both methods demonstrate septal enlargement in temporal lobe epilepsy.
- Septal thickness, which is easy to measure, could be a useful surrogate for septal volume

Introduction

Human septal nuclei are located in basal forebrain under and contiguous with the septum pellucidum. The septal nuclei, corresponding to the CH1-CH2 cell groups as defined by Mesulam (Mesulam et al., 1983; Zaborszky et al., 2008), include the ventrolateral, dorsolateral, intermediolateral, and septofimbrial nuclei, and medially, the vertical limb of the diagonal band of Broca (Andy and Stephan, 1968; Mai et al., 2004). The septal nuclei are strongly interconnected with the hippocampus via the fimbria/fornix (Amaral and Cowan, 1980; Colom, 2006; Mesulam et al., 1983; Saunders and Aggleton, 2007) and are essential for generating the hippocampal theta rhythm which is critical for learning and memory (Buzsaki, 2002; Gu and Yakel, 2011; Hangya et al., 2009; Huerta and Lisman, 1993; Stewart and Fox, 1990; Winson, 1978).

Despite their importance in normal cognition, as well as possible roles in human disorders including epilepsy and schizophrenia (Butler et al., 2013; Heath, 1961), human septal nuclei have received little research attention. This may relate to a persistent but incorrect belief that these nuclei are vestigial in humans (Andy and Stephan, 1968). The septal nuclei are not included in standard neuroanatomical parcellation schemes typically used to interpret human neuroimaging studies (Fischl et al., 2002; Tzourio-Mazoyer et al., 2002).

In response to this neglect, Zaborszky et al have developed probabilistic maps of the septal nuclei and other basal forebrain subregions based on combined MRI and histology (Zaborszky et al., 2008). Digital images and 3D MRI of cell-stained histological sections from the magnocellular (putatively cholinergic) basal forebrain region of 10 human postmortem brains were reconstructed and morphed to a template brain (Collins et al., 1994). We recently used these probabilistic maps in association with the segmentation tool from Statistical Parametric Mapping (SPM) to demonstrate septal enlargement in patients with temporal lobe epilepsy (TLE) (Butler et al., 2013). We interpreted these results as evidence of compensatory, neuroplastic augmentation of the septal-hippocampal system – a system which is antiepileptic in animal models of TLE (Colom et al., 2006; Miller et al., 1994). These probabilistic maps have also been used to demonstrate alterations in the size of basal forebrain subregions in association with normal cognition (Butler et al., 2012) and Alzheimer's Disease (Grothe et al., 2010).

However, volume measurements of the septal nuclei obtained with probabilistic maps have not been validated against manual tracing of high-resolution MRI. Manual tracing has traditionally been considered the gold standard for delineating brain structures on MRI. We therefore developed a protocol for manual tracing of the human septal region. The protocol is based on examination neuroanatomical specimens. Here, we (1) present our septal tracing protocol for 3D MRI acquired or reformatted in coronal sections, (2) report its inter-observer

reliability, (3) compare septal measurements obtained via manual tracing to those obtained automatically using probabilistic maps and Dartel toolbox in SPM, and (4) confirm that our prior finding of septal enlargement in TLE obtained using automatic methods (Butler et al., 2013) is also detectable using manual tracing.

Figure 1. Example of CH1-CH2 (septal) delineation on 200-um-thick coronal cresyl violet-stained sections of the formalin-fixed, celloidin-embedded brain from a 52 year old male who died without neurological disease. **A:** hemispheric section at the level of the globus pallidus (GP), caudate nucleus (CN) and putamen (Pu). The contours of the CH1 and CH2 nuclei are outlined in white. Because the major portion of the CH1 and CH2 septal nuclei is located on the level of the globus pallidus, the anterior GP extent has been used as a landmark for MRI tracing protocol. Note the strictly medial location of these nuclei. **B.** Low magnification (lens 2.5x) view of region demarcated by black rectangle in Panel A. **C.** Medium magnification (lens 40x) view to verify topography, borders and cytoarchitecture of CH1 and CH2 nuclei. CH1 (top) is composed mainly of small to medium size round neurons, whereas CH2 (bottom) has larger hyperchromatic neurons with prominent nucleus and dark nucleolus.

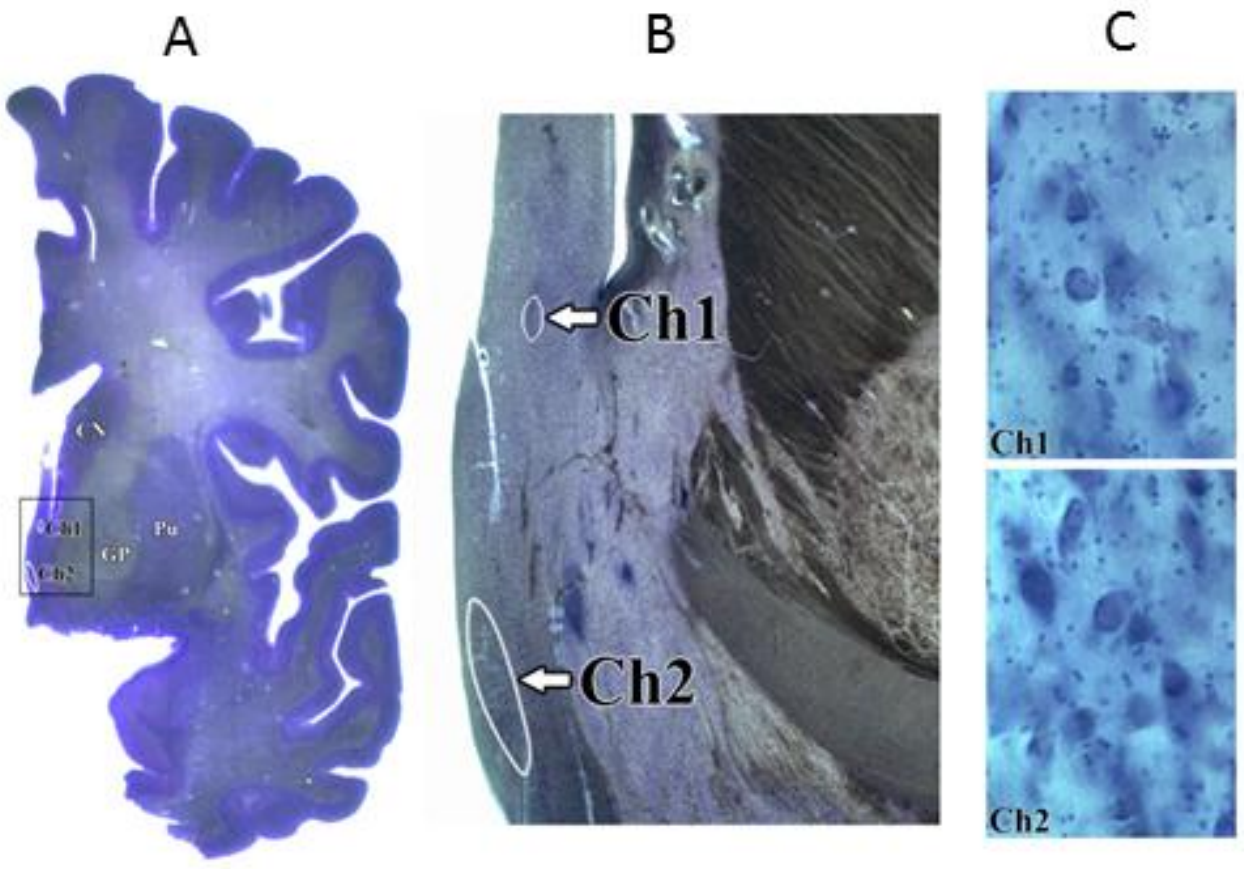

Materials and Methods

MRI Subjects

The MRI subjects in this IRB approved study were 14 patients with TLE (9 female; mean age:36.79, range:18.2-50.9, sd:10.74) receiving care at the NYU Comprehensive Epilepsy Center, and 72 normal controls (37 female; mean age: 33.73, range:19-64.1, sd: 12.41) recruited through advertisement. Patients and controls did not differ by age or sex. TLE was diagnosed by a board-certified neurologist based on standard clinical criteria including EEG and seizure semiology. Patients with TLE had a mean epilepsy duration of 18 years (range 2-43; sd 15.32). 5 patients had right-sided TLE, 8 had left-sided TLE, and 1 had bilateral TLE. No patients had any clinically significant neuroanatomical abnormality such as mesial temporal sclerosis, tumour, or other lesion, as determined by a board-certified neurologist or neuroradiologist. Some of these subjects were used in a prior study (Butler et al., 2013).

MRI Acquisition

High resolution T1-weighted scans were acquired sagitally at the NYU Center for Brain Imaging on a 3T Siemens Allegra head-only scanner. We used an MPRAGE sequence with parameters TE=3.25ms, TR=2530ms, TI=1100ms, flip angle=7.0 degrees, matrix 256x256x128, FOV=256x256x170.24mm, voxel size=1x1x1.33mm.

Examination of Brain Specimens:

Our protocol for manual delineation of the septal region on MRI was developed through examination of normal human brain specimens from the Institute for Basic Research (IBR) brain bank located in Staten Island, NY, with reference to probabilistic maps based on histology (Zaborszky et al., 2008), an atlas (Mai et al., 2004), and two prior publications (Callen et al., 2001; Vogels et al., 1990). Interaction between histology and MRI experts allowed identification of key features, visible both histologically and on MRI, that could be used as landmarks for an accurate and reliable protocol to trace septal nuclei on MRI.

Serial sections from 14 brains of subjects without records of neurological disorders, 10 males and four females, were preserved for postmortem studies. The cause of death of were traumatic multiple injuries (6 cases); drowning and electrocution (2 cases); myocardial infarct, cardiac arrest, or lymphocytic myocarditis (5 cases), bronchopneumonia (1 case). The postmortem interval (PMI), corresponding to the period between death and autopsy, ranged from 6 to 28 h (16.7 h on average; standard deviation ± 6.6 h). The average weight of the brains was 1,372 (± 118) grams. The brain hemisphere was fixed with 10% buffered formalin for an average of 408 days. Hemispheres were dehydrated in a series of ascending concentrations of ethyl alcohol. The average time

of dehydration was 38 (± 7) days. Dehydration was associated with reduction of brain hemisphere weight by 45% (± 7%). Brain hemispheres were embedded in 8% celloidin (Heinsen et al., 2000). Serial 200-µm-thick sections were stained with cresyl violet and mounted with Acrytol.

Delination of Ch1 and Ch2 nuclei. Every third section was used for delineation of the boundaries of the Ch1 and Ch2 (septal) nuclei. These two nuclei are the only portions of the magnocellular basal complex located within septum verum. Septum verum is well developed in the human brain contrary to the dorsally located septum pellucidum (Andy and Stephan, 1968). **Figure 1** is provided as an example to illustrate the topography of the Ch1 and Ch2 nuclei within the median septum verum as well as their size, shape and cytoarchitecture. In cresyl violet staining Ch1 and Ch2 neurons stand out sharply from their surroundings due their size and intense staining of their Nissl material. CH1 is composed mainly of small to medium size round neurons, whereas CH2 is composed mainly of larger hyperchromatic neurons with prominent nucleus and dark nucleolus. Ch1 (medial septal nucleus with approximately 10% of cholinergic neurons) boundaries are defined by small-sized neurons in the septum verum (dorsal and lateral border) and the diagonal band of Broca (ventral border). Dorsally, the Ch2 group (vertical limb nucleus of the diagonal band of Broca with approximately 70% of cholinergic neurons) borders with Ch1, medially with subarachnoidal space, and laterally with nucleus accumbens. Caudally Ch2 extends to the level of the globus pallidus (GP) (Vogels et al., 1990). Because the major portion of CH2 is detected at the level of the GP, the anterior GP extent – which is typically quite distinct on MRI – was chosen as the anterior landmark for beginning to trace septal nuclei on coronal MRI. Because septal nuclei borders the wall of lateral ventricle (see Figure 1), we chose a vertical line through the most medial border of each lateral ventricle as an MRI-visible lateral boundary. See below for details of manual tracing protocol.

Manual delineation of septal volume on MRI

Tracing was performed on de-identified MRI's by two independent, experienced tracers. One tracer traced all patient and control scans (n=86), and the other traced a random subset of 20 control scans. Tracing was performed using Firevoxel (Mikheev et al., 2008) on scans reformatted to coronal planes and perpendicular to the AC-PC line. Coronal slices were traced from anterior to posterior.

Figure 2. Manual definition of septal region on T1 template in MNI space (Collins et al., 1994) with tracing protocol landmarks shown. The *y* coordinates indicate distances from the anterior commissure in mm in the rostro-caudal directions. The left hemisphere is left in the image. The septal region on the template is present on four 1 mm thick coronal slices (B,C,D,E) and is shaded in red. **A.** Slice anterior to the septal nuclei in which globus pallidus is not visible and no septal gray matter is apparent. **B.** 1st slice traced in which the most anterior portion of septal region, shaded in red, is defined by the anterior-most appearance of bilateral globus pallidus (blue arrows, labeled GP). **C.** 2nd slice traced in which the crossing fibers of the anterior commissure (green arrow, labeled AC) are incompletely visualized. . **D.** 3rd slice traced in which crossing fibers of the anterior commissure (green arrow) are again visible but still appear incomplete medially. Yellow lines show the maximal septal thickness measurement. **E.** 4th and final slice traced. Because the anterior commissure is fully visible in this slice (green arrow), it serves as the inferior border of tracing. **F.** This slice was not considered to include any septal gray matter because the region had intensity identical to white matter, and CSF (purple arrow) was visible between the columns of the fornix. See text for details of tracing rules.

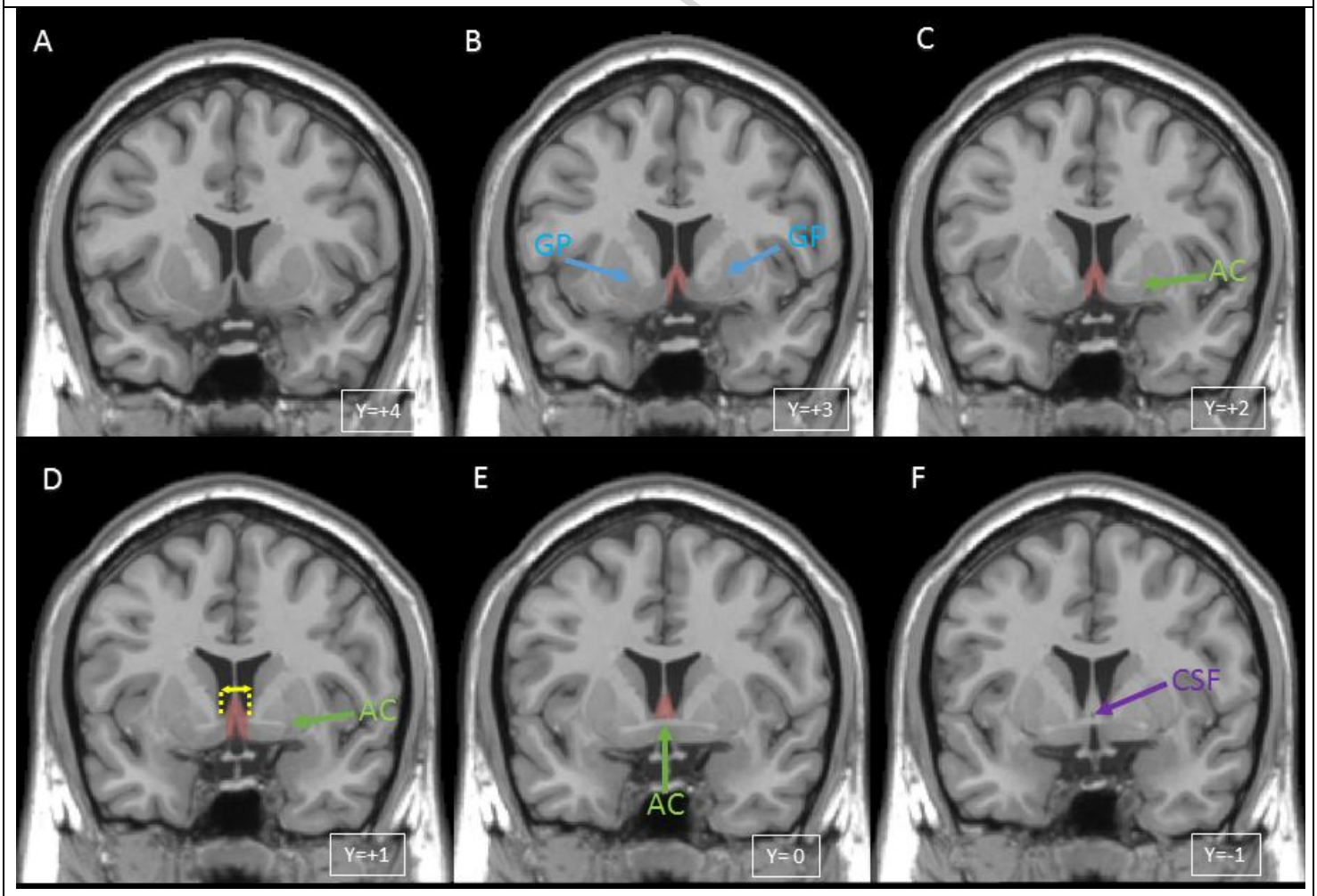

Tracing protocol

The anterior boundary was defined as the most anterior coronal slice in which bilateral globus pallidus was visible and gray matter at the base of the septum pellucidum was present (**Figure 2B**).
The superior extent of septal nuclei was defined as the point where the thin, membranous septum pellucidum widens into septal nuclei. Lateral boundaries were defined by parallel vertical lines through the most inferior and medial aspect of each lateral ventricle. These lateral boundaries are slightly more medial than those used in a prior study (Callen et al., 2001) but better match the narrow, medially-focused distribution of the CH1-CH2 cell group in anatomical specimens (Mai et al., 2004; Zaborszky et al., 2008) and as shown in **Figure 1**.
When a slice was anterior to the crossing fibers of the anterior commissure, the inferior boundary was the base of the brain, as in a prior protocol (Callen et al., 2001) and as shown in **Figure 2 B-D**. When the crossing fibers of the anterior commissure were fully visible, they served as the inferior boundary, as shown in **Figure 2E.**
The posterior boundary was defined by the following rule: A slice was considered to contain septal gray matter if it met at least two of the following three criteria: (1) the septal region still had gray (rather than white) matter intensity; (2) some or all of the crossing fibers of the anterior commissure were visible; (3) no CSF space in the center of the septal region (corresponding to CSF space between columns of the fornix) was visible. A slice NOT meeting these criteria is shown in **Figure 2F**.

We used these boundaries and landmarks to create an overinclusive, generally rectangular region of interest (ROI) from which CSF voxels (defined as having intensity less than half the average intensity of white matter as calculated by Firevoxel) were automatically removed to create the actual septal ROI (see Supplementary Materials for details of this optional automatic thresholding step; preliminary analyses indicated that including this automatic step in the protocol produced results nearly identical to those obtained using fully manual tracing while halving tracing time.) ROI volume in mm^3 was calculated and recorded
In addition, in order to determine if a manual tracing measure other than total volume might serve as a simple-to-measure surrogate for septal size, we recorded maximum septal thickness between the lateral ventricles (as shown in **Figure 2D**).

Automated Measurement of septal volume on MRI

Using Statistical Parametric Mapping (SPM8, Wellcome Trust Center for Neuroimaging) individual scans were normalized to the MNI152 T1-template using a 12-parameter affine transformation and partitioned into gray and white matter using a unified segmentation approach. Gray and white matter maps were registered to the segmented MNI152 T1-template using the DARTEL toolbox, an efficient large deformation diffeomorphic framework which provides information about voxel-level local expansion and contraction necessary to deform

the image to match the template.(Ashburner, 2007) The DARTEL flow fields derived from this registration were applied to a binary mask of the septal nuclei (generated as described below). To warp the septal maps, which were in MNI template space, back to each individual subject's native space, we applied the inverse DARTEL flow field. We then calculated the volume of each subject's septal mask in mm3. This method was used in our prior studies (Butler et al., 2012; Butler et al., 2013).

The binary septal nuclei masks were based on probabilistic maps of magnocellular (presumably cholinergic) basal forebrain cell groups generated using digital images of cell-stained histological sections from 10 human postmortem brains. The sections were reconstructed in 3D using the MRI scans of the fixed brain as a shape reference, then spatially normalized to the single-subject T1-weighted MNI reference brain, as described in detail elsewhere (Zaborszky et al., 2008). The masks included all voxels showing ≥50% probability of being part of the medial septal nucleus or the nucleus of the diagonal band of Broca, corresponding to Mesulam's Ch1-Ch2 cell group (Mesulam et al., 1983; Zaborszky et al., 2008).

To allow correction for differences in head size across subjects, total intracranial volume (TICV) was calculated from each MRI using Freesurfer 5.0 (http://surfer.nmr.mgh.harvard.edu).

Statistical Analysis

To assess inter-rater reliability, 20 scans from the control subjects were selected at random and manually traced by two individuals. The intraclass correlation coefficients (ICC) were computed between the two tracers for volume and maximum thickness using one-way random effects models. To assess agreement between manual and automated volume, we assessed the Pearson's correlation between these measures. We also assessed the Pearson's correlation between manual septal thickness (a potential surrogate for septal size) and manual and automated septal volume. These correlations were assessed in the entire subject group (n=86) as well as separately in patients (n=14) and controls (n=72). All of the brain measures were evaluated to confirm that they did not violate the assumptions of normality and linearity.

To compare manual and automated septal measures between controls and patients with TLE, ANCOVA was performed with TICV as a covariate to control for head size variability. These group analyses were performed with and without potential outliers, and with and without age as an additional covariate.

Results were considered significant at $p<.05$. Analyses were performed in IBM SPSS version 20.

Results

Average manual and automated septal measures for patients and controls are presented in **Table 1**. An example of the septal region as defined by manual tracing and automated procedures in a control subjects is shown in **Figure 3.**

Table 1. Mean, standard deviation and range of automated and manual septal measurements for TLE patients and controls.

	Automated septal volume (mm3)	Manual septal volume (mm3)	Manual septal thickness (mm)
TLE (n=14)	481.57 (79.80; 375-629)	327.93 (97.12; 163-477)	7.71 (1.20; 6-10)
Controls (n=72)	470.96 (58.01; 294-601)	289.4 (86.59; 128-508)	7.49 (1.41; 5-12)

Figure 3. Colocalization of manual and automated septal ROI's in a control subject. Manual ROI is yellow, automated ROI is blue, and overlap is green. The automated ROI extends several slices anterior and posterior to those presented, with only a small number of voxels on each of these slices.

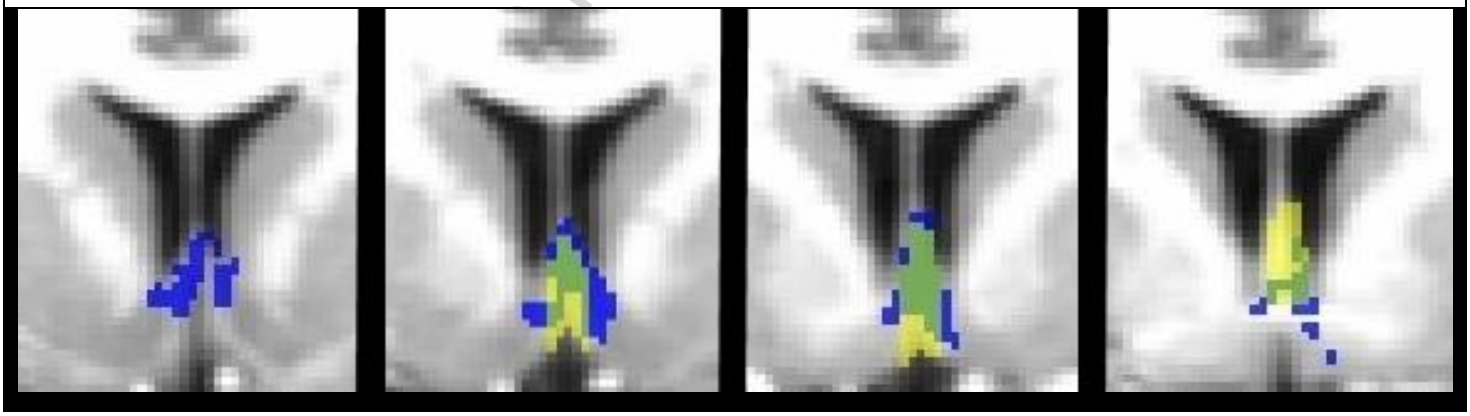

Inter-rater reliability of manual tracing protocol

ICC for the two tracers, each of whom traced 20 randomly selected control scans, was .767 ($p<.001$) for volume, and .780 ($p<.001$) for thickness.

Agreement between manual and automated volume measurement

Manual and automated volume were significantly correlated in the group as a whole ($R=.416$, $p<.001$, **Figure 4**), and in patients and controls separately (TLE: $R=.658$, $p=.010$; controls: $R=.344$, $p=.003$.)

Relation between manual septal thickness – a potential surrogate for septal volume - and manual and automated septal volume

Septal thickness was significantly correlated with both manual and automated septal volume in the group as a whole (manual: R=.289, p=.007; automated: R =.580, p<.001) and in patients and controls separately (TLE manual: R= .546, p=.043; TLE automated: R= .659, p=.010; control manual: R=.239, p=.043; control automated: R=.572, p<.001).

Figure 4. Plot showing correlation of manual and automatic septal measurements in patients and controls.

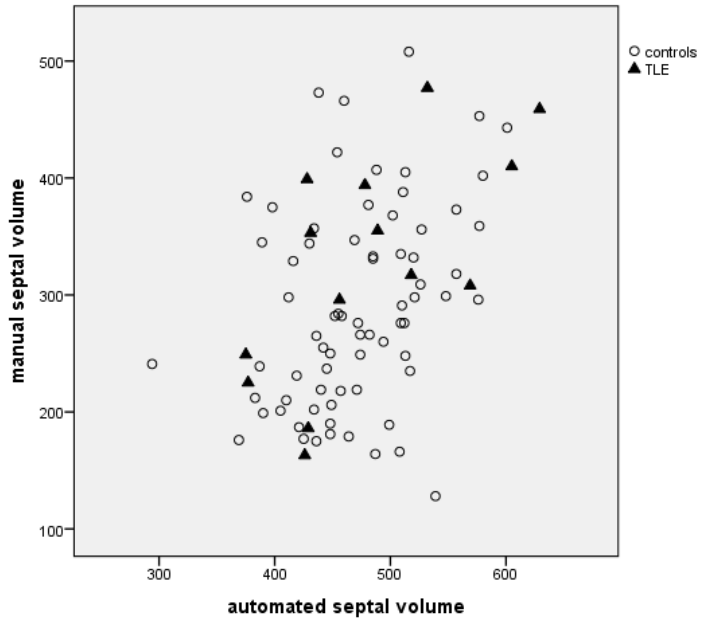

Group comparisons

TLE patients were found to have significantly greater septal volume than controls using both manual tracing (F[2,83]=4.637, p=.034) and automated measurement (F[2,83]=7.146, p=.009). Average patient and control septal volumes are presented in **Table 2.** Results were unchanged when age was included as an additional covariate and/or when outliers (two normal subjects, one with TICV two standard deviations below the mean, another with septal volume 2 standard deviations below the mean) were excluded.

Discussion

The septal nuclei are critical for learning and memory but have been the focus of relatively few human neuroimaging studies, likely because researchers and clinicians lack tools for accurately quantifying this region. Here, we describe a protocol for manual MRI delineation of human septal nuclei based on examination of neuroanatomical specimens, and we demonstrate that this protocol provides a reliable measure of septal volume. While manual septal volume measurements obtained using our new tracing protocol were reliable and correlated significantly with volumes computed automatically using probabilistic maps and SPM, the correlation was fairly low (.416). Studies comparing manual and automated volume measurements of other brain regions such as the hippocampus have shown much higher manual-automated correlations ranging from .6 to .9 (Hsu et al., 2002; Morey et al., 2009). The relatively poor manual-automated correlation in the current study indicates that manual and automated septal measures are not interchangeable, and suggests these two measures may be sensitive to different aspects of septal size. Differences between manual and automated measurements are obvious when inspecting the ROIs generated by each method shown in **Figure 3**: automatically-generated septal ROI's are irregular in shape and extend up to 14mm in anterior posterior extent, though with only one or a few voxels present on the most anterior and posterior slices. This voxel-by-voxel irregularity, to some extent a general feature of voxel-based automated methods, appears to be especially pronounced in the septal region. This may be because septal nuclei are comprised of small, dispersed neuronal groups embedded within white matter (Mai et al., 2004; Zaborszky et al., 2008), which gives the septal region a somewhat higher average image intensity (closer to white matter) than other gray matter regions, making accurate segmentation more challenging. In contrast, manual tracing relies upon human visualization of structure boundaries on distinct slices, necessitating smooth contours and sharp anterior and posterior boundaries. It is not surprising that these very different types of ROI's produced nonidentical volume measures. We interpret present results as demonstrating that manual and automated septal measures are highly congruant, though not identical. Providing important support for this congruance, patients with TLE were found to have significantly enlarged septal nuclei by both automated and manual methods. More generally, our results highlight that manual tracing and automated segmentation can provide complementary information, and performing both, especially for small and still-poorly-studied structures such as the septal nuclei, is important.

Septal MRI volumes in this study, whether measured manually or automatically, were less than half that of tissue shrinkage-corrected septal volume measured in post-mortem brains in a prior study of subjects with affective disorder, schizophrenia and controls. (Brisch et al., 2007) We believe this discrepancy relates primarily to different anatomical definitions of the septal region. In the present study, we delineate only a portion of the septum verum, while in the Brisch et al study, more anterior, posterior and lateral portions of the septal region are included. Ambiguity in delineating structures in this area of the brain are well known, and

reflected in the still-used term, substantia innominata. It will be interesting to determine whether abnormalities in the septal region in brains from schizophrenic patients, demonstrated in this (Brisch et al., 2007) and other (Heath, 1961) studies, are detectable via MRI.

Septal Thickness: We show that a very simple measure – maximal septal thickness between the ventricles – allows excellent inter-rater reliability, and correlates well with septal volume whether measured by manual or automated methods. Septal thickness may therefore be a simple, easily-measured characteristic that can be assessed in future studies; it could, for example, serve as a manual check of automated results, or as a standalone measure in clinical or other studies in which volume calculations are infeasible. However, septal thickness did not differ significantly between TLE patients and controls , suggesting it may be a less sensitive measure. Note that the septal thickness measurement does not relate to measures of cortical thickness derived using software such as Freesurfer. Cortical thickness refers specifically to the automatically-measured distance between the gray-white cortical junction and the pial surface of cortical gray matter, while septal thickness is a manual measure, corresponding to the thickness of the septal region between the ventricles. Because it requires only that the septum be visually distinguishable from surrounding CSF, it should be fairly insensitive to MRI acquisition variability, and therefore potentially appropriate for a wide range of studies.

Results provide additional support for a role of septal nuclei in epilepsy. As discussed in detail elsewhere (Butler et al., 2013), septal nuclei are strongly connected to hippocampi, and serve to dampen hippocampal hyperexcitability in animal models of TLE (Colom et al., 2006; Miller et al., 1994). We interpret our finding of septal enlargement specifically in TLE, obtained using both manual tracing and automated methods, as evidence that this antiepileptic septal-hippocampal system may be augmented in human TLE. It should be noted that our prior study (Butler et al., 2013) used 10% probabilistic maps whereas the current study used smaller, more specific, 50% masks; congruent results using these different masks again supports the robustness of our findings. A potential mechanism for septal enlargement in TLE is seizure-related increased retrograde transport of Nerve Growth Factor (NGF) from hippocampus to septum. NGF is essential for septal cholinergic neuron growth and survival, is supplied almost exclusively by hippocampus, and is highly upregulated by seizures (Gall and Isackson, 1989; Hagg et al., 1989; Hefti, 1986). Better understanding of this understudied, naturally-antiepileptic neural system could one day lead to better treatments for human TLE.

Limitations

This study focuses on validating measurement of septal nuclei – the CH1-CH2 portion of basal forebrain which is highly connected to hippocampus, and thus especially relevant to hippocampal diseases such as TLE; future studies can address other cell groups such as CH4 (the nucleus basalis of Meynert) implicated in disorders such as Alzheimer's Disease. Both automatic and manual methods could be insensitive to subregional variations in septal size (e.g. if the anterior septum enlarged while posterior septum degenerated, no overall volume difference would be detected.) To assess for such possibilities, analyses sensitive to shape variations might be helpful (Gerig et al., 2001).

In conclusion, we have developed a reliable manual tracing protocol based on human neuroanatomical specimens to measure septal volume, and compared it to automated methods. Our results highlight that manual tracing and automated segmentation of the human septal region provide complementary information, and call attention to the important though understudied human septal region which may play a key role in human diseases including epilepsy.

Figure Legends

Figure 1. Example of CH1-CH2 (septal) delineation on 200-um-thick coronal cresyl violet-stained sections of the formalin-fixed, celloidin-embedded brain from a 52 year old male who died without neurological disease. **A:** hemispheric section at the level of the globus pallidus (GP), caudate nucleus (CN) and putamen (Pu). The contours of the CH1 and CH2 nuclei are outlined in white. Because the major portion of the CH1 and CH2 septal nuclei is located on the level of the globus pallidus, the anterior GP extent has been used as a landmark for MRI tracing protocol. Note the strictly medial location of these nuclei. **B.** Low magnification (lens 2.5x) view of region demarcated by black rectangle in Panel A. **C.** Medium magnification (lens 40x) view to verify topography, borders and cytoarchitecture of CH1 and CH2 nuclei. CH1 (top) is composed mainly of small to medium size round neurons, whereas CH2 (bottom) has larger hyperchromatic neurons with prominent nucleus and dark nucleolus.

Figure 2. Manual definition of septal region on T1 template in MNI space (Collins et al., 1994) with tracing protocol landmarks shown. The *y* coordinates indicate distances from the anterior commissure in mm in the rostro-caudal directions. The left hemisphere is left in the image. The septal region on the template is present on four 1 mm thick coronal slices (B,C,D,E) and is shaded in red. **A.** Slice anterior to the septal nuclei in which globus pallidus is not visible and no septal gray matter is apparent. **B.** 1st slice traced in which the most anterior portion of septal region, shaded in red, is defined by the anterior-most appearance of bilateral globus pallidus (blue arrows, labeled GP). **C.** 2nd slice traced in which the crossing fibers of the anterior commissure (green arrow, labeled AC) are incompletely visualized. . **D.** 3rd slice traced in which crossing fibers of the anterior commissure (green arrow) are again visible but still appear incomplete medially. Yellow lines show the maximal septal thickness measurement. **E.** 4th and final slice traced. Because the anterior commissure is fully visible in this slice (green arrow), it serves as the inferior border of tracing. **F.** This slice was not considered to include any septal gray matter because the region had intensity identical to white matter, and CSF (purple arrow) was visible between the columns of the fornix. See text for details of tracing rules.

Figure 3. Colocalization of manual and automated septal ROI's in a control subject. Manual ROI is yellow, automated ROI is blue, and overlap is green. The automated ROI extends several slices anterior and posterior to those presented, with only a small number of voxels on each of these slices.

Figure 4. Plot showing correlation of manual and automatic septal measurements in patients and controls.

Acknowledgements

This study was supported by the following NIH grants: RO1AG12101, RO1AG022374, CRR MO1RR0096, P30AG008051, UL1TR000038, NS057579, NS023945

Brains used in this study were obtained from the Brain and Tissue Bank for Developmental Disorders of the National Institute of Child Health and Human Development at the University of Maryland; Harvard Brain Tissue Resource Center, Belmont, MA, supported in part by PHS grant number R24-MH 068855, and the Brain and Tissue Bank at the New York State Institute for Basic Research in Developmental Disabilities, Staten Island, NY.

References

Amaral, D.G., Cowan, W.M., 1980. Subcortical afferents to the hippocampal formation in the monkey. Journal of Comparative Neurology 189, 573-591.
Andy, O.J., Stephan, H., 1968. The septum in the human brain. J Comp Neurol 133, 383-410.
Ashburner, J., 2007. A fast diffeomorphic image registration algorithm. NeuroImage 38, 95-113.
Brisch, R., Bernstein, H.-G., Krell, D., Stauch, R., Trübner, K., Dobrowolny, H., Kropf, S., Bielau, H., Bogerts, B., 2007. Volumetric analysis of septal region in schizophrenia and affective disorder. European archives of psychiatry and clinical neuroscience 257, 140-148.
Butler, T., Blackmon, K., Zaborszky, L., Wang, X., DuBois, J., Carlson, C., Barr, W.B., French, J., Devinsky, O., Kuzniecky, R., Halgren, E., Thesen, T., 2012. Volume of the Human Septal Forebrain Region Is a Predictor of Source Memory Accuracy. Journal of the International Neuropsychological Society 18, 157-161.
Butler, T., Zaborszky, L., Wang, X., McDonald, C.R., Blackmon, K., Quinn, B.T., DuBois, J., Carlson, C., Barr, W.B., French, J., 2013. Septal nuclei enlargement in human temporal lobe epilepsy without mesial temporal sclerosis. Neurology 80, 487-491.
Buzsaki, G., 2002. Theta Oscillations in the Hippocampus. Neuron 33, 325-340.
Callen, D., Black, S.E., Gao, F., Caldwell, C., Szalai, J., 2001. Beyond the hippocampus MRI volumetry confirms widespread limbic atrophy in AD. Neurology 57, 1669-1674.
Collins, D.L., Neelin, P., Peters, T.M., Evans, A.C., 1994. Automatic 3d Intersubject Registration of Mr Volumetric Data in Standardized Talairach Space. Journal of Computer Assisted Tomography 18, 192-205.
Colom, L.V., 2006. Septal networks: relevance to theta rhythm, epilepsy and Alzheimer's disease. Journal of Neurochemistry 96, 609-623.
Colom, L.V., Garcia-Hernandez, A., Castaneda, M.T., Perez-Cordova, M.G., Garrido-Sanabria, E.R., 2006. Septo-Hippocampal Networks in Chronically Epileptic Rats: Potential Antiepileptic Effects of Theta Rhythm Generation. Journal of Neurophysiology 95, 3645-3653.
Fischl, B., Salat, D.H., Busa, E., Albert, M., Dieterich, M., Haselgrove, C., van der Kouwe, A., Killiany, R., Kennedy, D., Klaveness, S., Montillo, A., Makris, N., Rosen, B., Dale, A.M., 2002. Whole brain segmentation: automated labeling of neuroanatomical structures in the human brain. Neuron 33, 341-355.
Gall, C., Isackson, P., 1989. Limbic seizures increase neuronal production of messenger RNA for nerve growth factor. Science 245, 758-761.
Gerig, G., Styner, M., Shenton, M.E., Lieberman, J.A., 2001. Shape versus size: Improved understanding of the morphology of brain structures. Medical Image Computing and Computer-Assisted Intervention–MICCAI 2001. Springer, pp. 24-32.

Grothe, M., Zaborszky, L., Atienza, M., Gil-Neciga, E., Rodriguez-Romero, R., Teipel, S.J., Amunts, K., Suarez-Gonzalez, A., Cantero, J.L., 2010. Reduction of basal forebrain cholinergic system parallels cognitive impairment in patients at high risk of developing Alzheimer's disease. Cerebral Cortex 20, 1685-1695.
Gu, Z., Yakel, J., 2011. Timing-Dependent Septal Cholinergic Induction of Dynamic Hippocampal Synaptic Plasticity. Neuron 71, 155-165.
Hagg, T., Fass-Holmes, B., Vahlsing, H.L., Manthorpe, M., Conner, J.M., Varon, S., 1989. Nerve growth factor (NGF) reverses axotomy-induced decreases in choline acetyltransferase, NGF receptor and size of medial septum cholinergic neurons. Brain Res 505, 29-38.
Hangya, B., Borhegyi, Z., Szilagyi, N., Freund, T., Varga, V., 2009. GABAergic Neurons of the Medial Septum Lead the Hippocampal Network during Theta Activity. The Journal of Neuroscience 29, 8094-8102.
Heath, R.G., 1961. Common characteristics of epilepsy and schizophrenia: clinical observation and depth electrode studies. 1961. reprinted in Epilepsy Behav 6, 633-645.
Hefti, F., 1986. Nerve growth factor promotes survival of septal cholinergic neurons after fimbrial transections. The Journal of Neuroscience 6, 2155-2162.
Heinsen, H., Arzberger, T., Schmitz, C., 2000. Celloidin mounting (embedding without infiltration)—a new, simple and reliable method for producing serial sections of high thickness through complete human brains and its application to stereological and immunohistochemical investigations. Journal of chemical neuroanatomy 20, 49-59.
Hsu, Y.Y., Schuff, N., Du, A.T., Mark, K., Zhu, X., Hardin, D., Weiner, M.W., 2002. Comparison of automated and manual MRI volumetry of hippocampus in normal aging and dementia. Journal of Magnetic Resonance Imaging 16, 305-310.
Huerta, P.T., Lisman, J.E., 1993. Heightened synaptic plasticity of hippocampal CA1 neurons during a cholinergically induced rhythmic state. Nature 364, 723-725.
Mai, J., Assheuer, J., Paxinos, G., 2004. Atlas of the human brain. Elsevier Academic Press, Boston :.
Mesulam, M.M., Mufson, E.J., Wainer, B.H., Levey, A.I., 1983. Central cholinergic pathways in the rat: an overview based on an alternative nomenclature (Ch1-Ch6). Neuroscience 10, 1185-1201.
Mikheev, A., Nevsky, G., Govindan, S., Grossman, R., Rusinek, H., 2008. Fully automatic segmentation of the brain from T1-weighted MRI using Bridge Burner algorithm. Journal of Magnetic Resonance Imaging 27, 1235-1241.
Miller, J.W., Turner, G.M., Gray, B.C., 1994. Anticonvulsant effects of the experimental induction of hippocampal theta activity. Epilepsy Research 18, 195-204.
Morey, R.A., Petty, C.M., Xu, Y., Pannu Hayes, J., Wagner Ii, H.R., Lewis, D.V., LaBar, K.S., Styner, M., McCarthy, G., 2009. A comparison of automated segmentation and manual tracing for quantifying hippocampal and amygdala volumes. NeuroImage 45, 855-866.
Saunders, R.C., Aggleton, J.P., 2007. Origin and topography of fibers contributing to the fornix in macaque monkeys. Hippocampus 17, 396-411.
Stewart, M., Fox, S.E., 1990. Do septal neurons pace the hippocampal theta rhythm? Trends in Neurosciences 13, 163-169.
Tzourio-Mazoyer, N., Landeau, B., Papathanassiou, D., Crivello, F., Etard, O., Delcroix, N., Mazoyer, B., Joliot, M., 2002. Automated anatomical labeling of activations in SPM using a macroscopic anatomical parcellation of the MNI MRI single-subject brain. NeuroImage 15, 273-289.
Vogels, O., Broere, C., Ter Laak, H., Ten Donkelaar, H., Nieuwenhuys, R., Schulte, B., 1990. Cell loss and shrinkage in the nucleus basalis Meynert complex in Alzheimer's disease. Neurobiology of aging 11, 3-13.
Winson, J., 1978. Loss of hippocampal theta rhythm results in spatial memory deficit in the rat. Science 201, 160-163.
Zaborszky, L., Hoemke, L., Mohlberg, H., Schleicher, A., Amunts, K., Zilles, K., 2008. Stereotaxic probabilistic maps of the magnocellular cell groups in human basal forebrain. NeuroImage 42, 1127-1141.